Biomaterials Science

ROYAL SOCIETY OF CHEMISTRY

PAPER

View Article Online
View Journal | View Issue

Check for updates

Cite this: *Biomater. Sci.*, 2023, **11**, 2870

Structural optimization of BODIPY photosensitizers for enhanced photodynamic antibacterial activities†

Hui Wen,[a,b] Qihang Wu,[a,b] Liqian Liu,[a,b] Yite Li,[a,b] Tingting Sun *[a] and Zhigang Xie *[a,b]

Received 16th January 2023,
Accepted 16th February 2023

DOI: 10.1039/d3bm00073g

rsc.li/biomaterials-science

Enhancing the interactions between photosensitizers and bacteria is key to developing effective photodynamic antibacterial agents. However, the influence of different structures on the therapeutic effects has not been systematically investigated. Herein, 4 BODIPYs with distinct functional groups, including the phenylboronic acid (PBA) group and pyridine (Py) cations, were designed to explore their photodynamic antibacterial activities. The BODIPY with the PBA group (IBDPPe-PBA) exhibits potent activity against planktonic *Staphylococcus aureus* (*S. aureus*) upon illumination, while the BODIPY with Py cations (IBDPPy-Ph) or both the PBA group and Py cations (IBDPPy-PBA) can significantly minimize the growth of both *S. aureus* and *Escherichia coli* (*E. coli*). In particular, IBDPPy-Ph can not only eliminate the mature *S. aureus* biofilm and *E. coli* biofilm *in vitro*, but also promote the healing of the infected wound. Our work provides an alternative for reasonable design of photodynamic antibacterial materials.

1. Introduction

Infectious diseases caused by pathogenic bacteria remain pressing threats to public health and are extremely difficult to cure because the complex membrane structures of bacteria can impede the penetration of drugs or other invaders.[1–6] In addition, the emergence and constant mutation of drug-fast bacteria ascribed to the overuse and frequent dosing of antibiotics exacerbate the problems.[7–10] Photodynamic therapy (PDT) is an emerging modality to treat pathogenic bacterial infections. In PDT, the excited photosensitizers (PSs) produce reactive oxygen species (ROS) such as singlet oxygen ($^1O_2$) species, which possess high toxicities.[11–15] What's more, the prominent advantages of PDT including non-invasiveness, high spatiotemporal selectivity, negligible systemic toxicity, and low drug resistance, make it one of the most important antibacterial strategies.[16–20] However, the inherent characteristics of $^1O_2$, such as the short lifetime and diffusion range, severely restrict the antimicrobial effects of PDT.[21] Therefore, development of efficient PSs to treat bacterial infections still requires constant exploration.

At present, the construction of antibacterial drugs is focused on enhancing their interactions toward bacteria for solving the dilemma.[22–26] The phenylboronic acid (PBA) group, as a common targeting group, can actively bind to lipopolysaccharide (LPS) and teichoic acid, the major components of the cell walls of Gram-negative (G−) and Gram-positive (G+) bacteria, respectively, *via* forming borate ester.[27–30] On the other hand, positively charged groups such as pyridine (Py) cations can attach to bacteria *via* the intense electrostatic attractions between the positively charged ligands and the negatively charged membrane regions of bacteria.[31–34] To date, numerous antibacterial PSs have achieved great therapeutic effects by utilizing either the targeting strategy or electrostatic interactions. Nevertheless, the antibacterial effects of these two binding modes have not been compared in more detail.[35–37]

In this work, the PBA group and Py cations were selected as the representatives of targeting function and electrostatic interaction, respectively, to systematically study their influence on photodynamic antibacterial activity. 4,4-Difluoro-4-bora-3a,4a-diaza-*s*-indacene (BODIPY) was selected as the PS for PDT of bacterial infections because of its excellent performances, such as the large molar absorption coefficients and the feasible modification.[38–41] The PBA group and Py cations were introduced into the BODIPY matrix individually or simultaneously to synthesize BODIPY PSs. They are nonfunctionalized BODIPY (IBDPPe-Ph), PBA-functionalized BODIPY (IBDPPe-PBA), Py cation-functionalized BODIPY (IBDPPy-Ph) and PBA and Py cation-functionalized BODIPY (IBDPPy-PBA), respectively (Fig. 1A). Then, the photodynamic antibacterial

[a]*State Key Laboratory of Polymer Physics and Chemistry, Changchun Institute of Applied Chemistry, Chinese Academy of Sciences, Changchun, Jilin 130022, P. R. China. E-mail: suntt@ciac.ac.cn, xiez@ciac.ac.cn*
[b]*University of Science and Technology of China, Hefei 230026, P. R. China*
†Electronic supplementary information (ESI) available: Experimental methods and supporting figures. See DOI: https://doi.org/10.1039/d3bm00073g

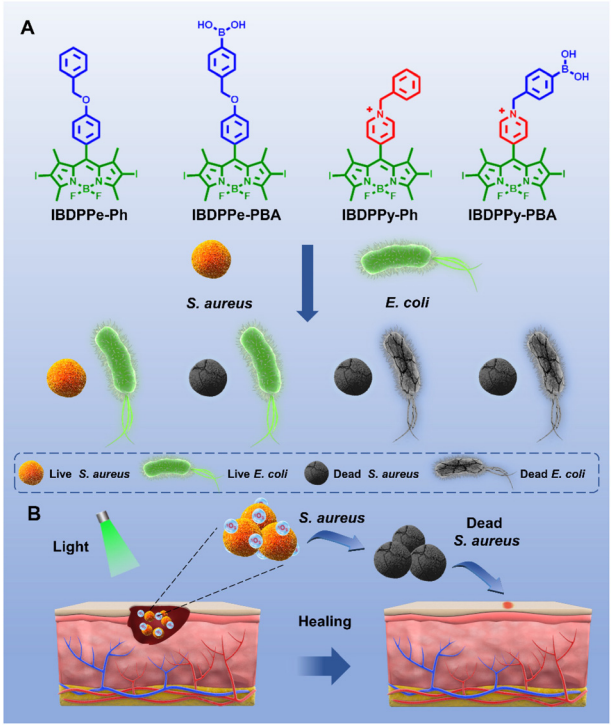

Fig. 1 (A) Structures of IBDPPe-Ph, IBDPPe-PBA, IBDPPy-Ph, and IBDPPy-PBA and the differences in antibacterial activities of the 4 BODIPYs toward *S. aureus* and *E. coli*. (B) Schematic illustration of the antibacterial application *in vivo*.

activities of the 4 BODIPYs toward *Staphylococcus aureus* (*S. aureus*) and *Escherichia coli* (*E. coli*) were comprehensively studied and compared *in vitro* and *in vivo* (Fig. 1).

2. Experimental section

2.1. Synthesis of IBDPPe-Ph

BDPPe was synthesized as the precursor *via* a previously reported method.[42] Caesium carbonate (300 mg) was added to a solution of BDPPe (51 mg, 0.15 mmol) and benzyl bromide (20 μL, 0.17 mmol) in dry tetrahydrofuran (THF, 6 mL). The solution was stirred at ambient temperature for 6 h under nitrogen. The solution was filtered, and the filtrate was evaporated to obtain the crude product. BDPPe-Ph was obtained after purification by silica gel column chromatography using *n*-hexane/CH_2Cl_2 (v/v = 1 : 1). Then, a solution of BDPPe-Ph (49 mg, 0.11 mmol) and *N*-iodosuccinimide (128 mg, 0.57 mmol) in CH_2Cl_2 (5 mL) was added to a dark flask. The mixed solution was stirred at ambient temperature for 6 h. The solution was evaporated to obtain the crude product. Finally, IBDPPe-Ph was obtained after purification by silica gel column chromatography with *n*-hexane/CH_2Cl_2 (v/v = 2 : 1) as the eluent.

2.2. Synthesis of IBDPPe-PBA

Caesium carbonate (300 mg) was added to a solution of BDPPe (51 mg, 0.15 mmol) and 4-(bromomethyl)phenylboronic acid pinacol cyclic ester (68 mg, 0.23 mmol) in dry THF (3 mL). The solution was stirred at ambient temperature overnight under nitrogen. The solution was filtered, and the filtrate was evaporated to obtain the crude product. The crude product was purified by silica gel column chromatography with *n*-hexane/CH_2Cl_2 (v/v = 1 : 5) as the eluent to obtain BDPPe-PBAP. Next, a solution of BDPPe-PBAP (36 mg, 0.07 mmol) and *N*-iodosuccinimide (88 mg, 0.40 mmol) in CH_2Cl_2 (3 mL) was added to a dark flask. The solution was stirred at ambient temperature overnight and evaporated to obtain the crude product. The crude product was purified by silica gel column chromatography with *n*-hexane/CH_2Cl_2 (v/v = 1 : 3) as the eluent to obtain IBDPPe-PBAP. Then, $NaIO_4$ (190 mg) in H_2O (1.5 mL) was added to a solution of IBDPPe-PBAP (44 mg, 0.55 mmol) and NH_4Cl (40 mg) in a mixed solvent (THF/H_2O (v/v) = 9 : 1, 10 mL). The mixed solution was stirred at ambient temperature for 24 h. After vacuum rotary evaporation to remove THF, the solution was filtered, and the precipitate was washed with H_2O (1 mL) several times and dried in a vacuum to obtain the crude product. Finally, IBDPPe-PBA was obtained after purification by silica gel column chromatography with CH_3OH/CH_2Cl_2 (v/v = 1 : 100) as the eluent.

2.3. Synthesis of IBDPPy-Ph

BDPPy was synthesized as the precursor *via* a previously reported method.[43] A solution of BDPPy (310 mg, 0.54 mmol) and *N*-iodosuccinimide (490 mg, 2.75 mmol) in CH_2Cl_2 (5 mL) was added to a dark flask. The solution was stirred at ambient temperature for 6 h, and the crude product was obtained *via* rotary evaporation. The crude product was purified by silica gel column chromatography with ethyl acetate/CH_2Cl_2 (v/v = 1 : 50) as the eluent to obtain IBDPPy.

Benzyl bromide (120 μL, 0.70 mmol) was added to a solution of IBDPPy (58 mg, 0.10 mmol) in dry toluene (10 mL). The solution was stirred at 110 °C overnight. Then the solution was filtered, and the precipitate was washed with toluene (1 mL) several times after cooling to room temperature. Finally, the precipitate was dried in a vacuum to obtain IBDPPy-Ph.

2.4. Synthesis of IBDPPy-PBA

4-(Bromomethyl)phenylboronic acid (34 mg, 0.12 mmol) was added to a solution of IBDPPy (58 mg, 0.10 mmol) in dry acetonitrile (10 mL). The solution was stirred at 75 °C for 24 h under nitrogen. Then, the solution was filtered, and the precipitate was washed with acetonitrile (1 mL) several times after cooling to room temperature. Finally, the precipitate was dried in a vacuum to obtain IBDPPy-PBA.

3. Results and discussion

3.1. Synthesis of BODIPYs

First, BDPPe and BDPPy were synthesized as the precursors *via* previously reported methods (Fig. S1 and S2†).[42,43] Then, various functional groups were introduced separately, and an iodine substitution reaction was carried out to boost the inter-

system crossing (ISC) for the generation of $^1O_2$.[44] The synthetic routes to IBDPPe-Ph, IBDPPe-PBA, IBDPPy-Ph, and IBDPPy-PBA are shown in Fig. S3–S6†, and their chemical structures are confirmed by ^{1}H nuclear magnetic resonance (^{1}H NMR) spectroscopy and electrospray ionization mass spectrometry (ESI-MS) (Fig. S7–S14†). In IBDPPe-PBA and IBDPPy-Ph, the PBA group and Py cations serve as the functional groups for enhancing the interactions between PSs and bacteria. In IBDPPy-PBA, both the PBA group and Py cations are introduced. Also, IBDPPe-Ph was synthesized as the control molecule.

3.2. Photophysical properties and $^1O_2$ generation capacities

The photophysical properties of the 4 BODIPYs were evaluated using absorption and fluorescence spectra. IBDPPe-Ph and IBDPPe-PBA have the same maximum absorption peaks at 535 nm, while IBDPPy-Ph and IBDPPy-PBA show absorption peaks at 550 nm in dimethyl sulfoxide (DMSO) (Fig. 2A). In addition, the fluorescence intensity of IBDPPy-Ph and IBDPPy-PBA is obviously lower than that of IBDPPe-Ph and IBDPPe-PBA (Fig. 2B), resulting from the low electron cloud density of pyridine.

Furthermore, the $^1O_2$ generation capacities of the 4 BODIPYs were investigated. 1,3-Diphenylisobenzofuran (DPBF) was selected as the indicator to monitor the generation of $^1O_2$ under green light irradiation. DPBF can react with $^1O_2$ and be converted to 1,2-dibenzoylbenzene, leading to a significant decrease in absorbance. In the presence of IBDPPy-Ph or IBDPPy-PBA, the absorbance of DPBF at 420 nm decreases faster than that with IBDPPe-Ph or IBDPPe-PBA (Fig. 2C and S15†). However, the absorbance of DPBF alone changes insignificantly under green light irradiation for 50 s. The results indicate that the $^1O_2$ generation abilities of IBDPPy-Ph and IBDPPy-PBA are higher than those of IBDPPe-Ph and IBDPPe-PBA.

To explain the spectroscopic properties of these BODIPYs, the energy gaps (ΔE) of the highest occupied molecular orbital (HOMO) and the lowest unoccupied molecular orbital (LUMO) as well as the singlet–triplet energy gaps (ΔE_{ST}) were calculated through density functional theory (DFT). The HOMO–LUMO distributions of the BODIPYs were calculated, and the ΔE values of IBDPPe-Ph, IBDPPe-PBA, IBDPPy-Ph and IBDPPy-PBA are 0.11, 0.10, 0.07, and 0.07 eV, respectively (Fig. S16†). As shown in Fig. 2D, the ΔE_{ST} values of IBDPPe-Ph, IBDPPe-PBA, IBDPPy-Ph, and IBDPPy-PBA are 1.27, 1.27, 0.22, and 0.24 eV, respectively. The smaller ΔE_{ST} values of IBDPPy-Ph and IBDPPy-PBA than those of IBDPPe-Ph and IBDPPe-PBA contribute to the ISC processes, thus promoting the generation of ROS, which is consistent with their $^1O_2$ generation capacities (Fig. 2D).[45,46]

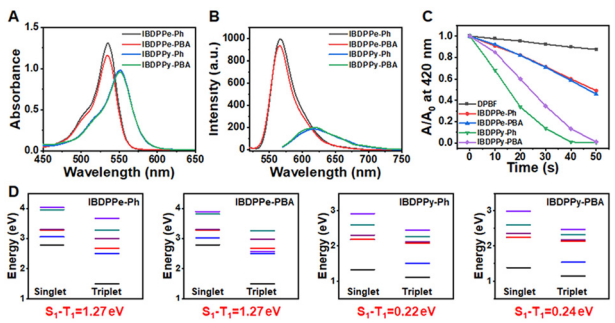

Fig. 2 Photophysical properties of the 4 BODIPYs. (A) Absorption and (B) fluorescence spectra of the 4 BODIPYs (15 μM) in DMSO. (C) $^1O_2$ generation of the 4 BODIPYs (2 μM) upon green light irradiation (18 mW cm^{-2}) with DPBF as the indicator. (D) The excited singlet and triplet distributions and the ΔE_{ST} values of 4 BODIPYs were calculated by DFT. Optimized with Gaussian 09/B3LYP/6-31G*.

3.3. *In vitro* antibacterial assays

To compare the influence of different functional ligands on the photodynamic antibacterial effects of PSs, the *in vitro* antibacterial activities of the 4 BODIPYs were studied. *S. aureus* and *E. coli* were selected as the representatives of G+ and G− bacteria, respectively, and green light irradiation was performed. As shown in Fig. 3A, at a low concentration of 0.5 μM, both IBDPPe-PBA and IBDPPy-PBA could almost completely inhibit the growth of *S. aureus*. The proliferation of *S. aureus* is also suppressed by IBDPPy-Ph at a concentration of 1 μM. However, IBDPPe-Ph does not exhibit an obvious antibacterial effect against *S. aureus* even at a high concentration of 3 μM. The minimal inhibitory concentrations (MICs) of IBDPPe-Ph, IBDPPe-PBA, IBDPPy-Ph, and IBDPPy-PBA toward *S. aureus* are determined to be 8, 0.3, 0.9, and 0.3 μM, respectively (Fig. S17†). As for *E. coli*, the Py cation-functionalized BODIPYs (IBDPPy-Ph and IBDPPy-PBA) show dramatic inhibition effects at a concentration of 5 μM under green light irradiation (Fig. 3B). However, the *E. coli* treated with IBDPPe-Ph or

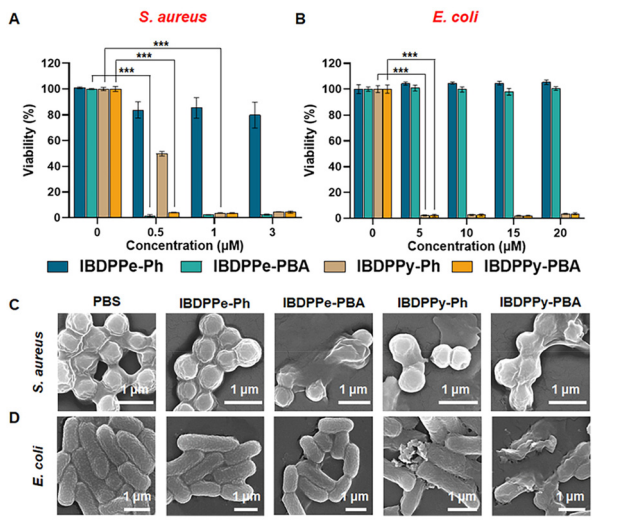

Fig. 3 Antibacterial activities of the BODIPYs. The *in vitro* bacterial viability of (A) *S. aureus* and (B) *E. coli* treated with different concentrations of IBDPPe-Ph, IBDPPe-PBA, IBDPPy-Ph, and IBDPPy-PBA under green light irradiation (18 mW cm^{-2}). (C) SEM images of *S. aureus* in the presence of IBDPPe-Ph, IBDPPe-PBA, IBDPPy-Ph, and IBDPPy-PBA (2 μM) under green light irradiation (18 mW cm^{-2}). (D) SEM images of *E. coli* treated with IBDPPe-Ph, IBDPPe-PBA, IBDPPy-Ph, and IBDPPy-PBA (15 μM) under green light irradiation (18 mW cm^{-2}). ***$p < 0.001$.

IBDPPe-PBA shows insignificant decrease in viability even at a concentration of 20 μM under green light irradiation. Then, the MICs of the 4 BODIPYs toward *E. coli* were further studied. The MICs of IBDPPy-Ph and IBDPPy-PBA are 2 and 3 μM, respectively, while those of IBDPPe-Ph and IBDPPe-PBA are not reached even at a concentration of 25 μM (Fig. S18†). These results revealed the great potential of Py cations in antibacterial agents.

Furthermore, the colony forming unit (CFU) plate counting method was used to verify the antibacterial results of BODIPYs against planktonic bacteria. The CFU counting results (Fig. S19 and S20†) are consistent with the antibacterial effects toward planktonic bacteria (Fig. 3A and B). In order to directly visualize the morphological changes of bacteria after illumination, scanning electron microscopy (SEM) was further employed. In Fig. 3C, the membranes of *S. aureus* treated with PBS or IBDPPe-Ph remain intact with clear and sharp edges, while those incubated with IBDPPe-PBA, IBDPPy-Ph, or IBDPPe-Ph exhibit visible shrinkage, fusion, splitting, and collapse. In addition, the *E. coli* treated with PBS, IBDPPe-Ph, or IBDPPe-PBA keep their initial morphologies with intact surfaces, while for those treated with IBDPPy-Ph or IBDPPy-PBA, distinct shrinkage, collapse, and fusion are observed (Fig. 3D), further demonstrating the strong interactions and good antibacterial activities of IBDPPy-Ph and IBDPPy-PBA toward *E. coli*.

The *in vitro* antibacterial assays directly prove that the BODIPY modified with the PBA group individually (IBDPPe-PBA) possesses powerful antibacterial activity against G+ bacteria selectively, while the Py cation-functionalized BODIPYs (IBDPPy-Ph and IBDPPy-PBA) show potent inhibition effects toward both G+ and G− bacteria. G+ bacteria only have a single lipid membrane, and the heavy peptidoglycan contains high levels of teichoic acid, providing a large number of binding sites for the antibacterial agents containing PBA groups. Different from G+ bacteria, the cell walls of the G− bacteria are composed of a double membrane, the outer membrane and the inner membrane. The presence of the outer membrane protein (OMP) and the inner membrane endows G− bacteria with high resistance to external invaders, including antibacterial agents.[47] In addition, an important commonality between both G+ and G− bacteria is that their envelopes are negatively charged. The cationic BODIPYs can be adsorbed on the negatively charged membranes, and then the amphiphilic nature of the BODIPYs can denature the OMP and perturb the lipid membranes *via* hydrophobic interactions.[48] Therefore, we speculate that the PBA group alone can bind with G+ or G− bacteria through the reactions with high levels of teichoic acid or LPS, but it is unable to break the barriers of the OMP and the inner membrane of G− bacteria. However, Py cations can adhere to both G+ and G− bacteria through electrostatic interactions and perturb the bacterial membrane *via* hydrophobic interactions (Fig. 4). In summary, PBA can serve as a powerful functional group to enhance the antibacterial activities of PSs against G+ bacteria, and Py cations can amplify the antibacterial effects of PSs toward both G+ and G− bacteria, which is consistent with the results from previous work.[49]

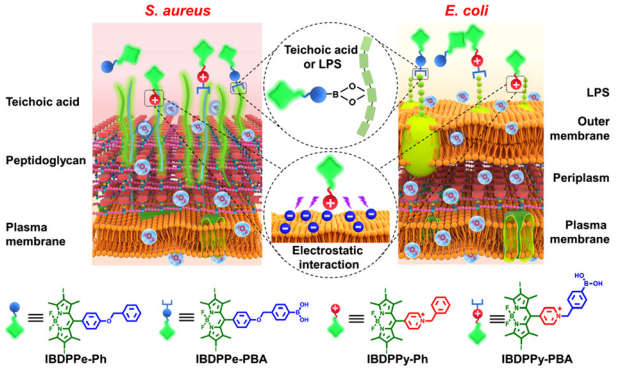

Fig. 4 Interactions between the PBA-functionalized BODIPYs and teichoic acid/LPS of bacteria *via* the borate ester covalent bond, as well as the electrostatic interactions between the Py cation-functionalized BODIPYs and the negatively charged membranes of bacteria.

3.4. Antibiofilm effects

Based on the excellent antibacterial potency of IBDPPy-PBA and IBDPPy-Ph toward planktonic bacteria, their bioactivities against *S. aureus* and *E. coli* biofilms were further explored. First, we quantified the biofilm mass *via* 3-(4,5-dimethyl-2-thiazolyl)-2,5-diphenyltetrazolium bromide (MTT) assay. *S. aureus* or *E. coli* were incubated with different concentrations of BODIPYs for 30 min, and treated with or without green light irradiation (18 mW cm^{-2}) for 10 min. Then, the biofilm formation was detected by MTT assay after static culture for 24 h. For *S. aureus* subjected to light irradiation, the formation of biofilms was gradually reduced with the increase in concentration of IBDPPy-PBA or IBDPPy-Ph, and it was completely inhibited by 1.25 μM IBDPPy-PBA or 1.5 μM IBDPPy-Ph (Fig. 5A). As for *E. coli*, similar phenomena were observed except that the biofilm formation was completely inhibited at higher concentrations (15 μM IBDPPy-PBA or 10 μM IBDPPy-Ph) (Fig. 5B). However, neither IBDPPy-PBA nor IBDPPy-Ph under dark conditions could inhibit the biofilm formation of *S. aureus* and *E. coli*.

Subsequently, the eradication capacities of IBDPPy-PBA and IBDPPy-Ph toward mature biofilms were studied. The mature biofilms of *S. aureus* and *E. coli* were incubated with different concentrations of IBDPPy-PBA or IBDPPy-Ph for 30 min, and then irradiated or not irradiated with green light for 10 min. Afterwards, the biofilm biomass was detected by MTT assay after static culture for 30 min. As shown in Fig. 5C and D, the eradication of mature biofilms by IBDPPy-PBA or IBDPPy-Ph is also dose-dependent. As depicted in Fig. 5C, IBDPPy-Ph at 30 μM exhibit a significantly better eradication effect toward *S. aureus* biofilms than IBDPPy-PBA either under dark or light conditions. Surprisingly, both IBDPPy-PBA and IBDPPy-Ph can eradicate *E. coli* biofilms at 2 μM upon green light irradiation.

The eradication capacities of IBDPPy-PBA and IBDPPy-Ph toward mature biofilms were also analyzed by staining with SYTO and propidium iodide (PI). Visible green fluorescence signals are observed in the confocal laser scanning microscopy

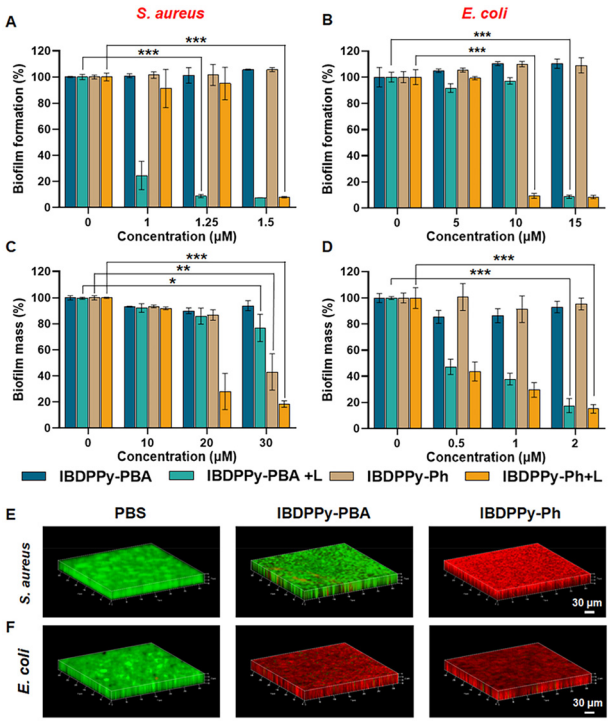

Fig. 5 Anti-biofilm effects of the BODIPYs. Biofilm formation of (A) *S. aureus* and (B) *E. coli* incubated with IBDPPy-PBA or IBDPPy-Ph with or without light irradiation. The biofilm masses of (C) *S. aureus* biofilms and (D) *E. coli* biofilms incubated with IBDPPy-PBA or IBDPPy-Ph with or without light irradiation. (E) 3D CLSM images of *S. aureus* biofilms incubated with PBS, IBDPPy-PBA, or IBDPPy-Ph (30 μM) under green light irradiation. (F) 3D CLSM images of *E. coli* biofilms incubated with PBS, IBDPPy-PBA or IBDPPy-Ph (2 μM) under green light irradiation. Power density of green light: 18 mW cm^{-2}. *$p < 0.05$, **$p < 0.01$, and ***$p < 0.001$.

(CLSM) images of the *S. aureus* biofilms treated with PBS or IBDPPy-PBA, which indicates that IBDPPy-PBA could not destroy the mature *S. aureus* biofilms either with or without irradiation (Fig. 5E and S21†). However, intense red fluorescence is observed in the CLSM image of the IBDPPy-Ph and light irradiation treated *S. aureus* biofilm, confirming that IBDPPy-Ph can penetrate and destroy the mature *S. aureus* biofilm under irradiation (Fig. 5E). Moreover, IBDPPy-Ph without light irradiation can also destroy the mature *S. aureus* biofilm to some extent, as demonstrated by the moderate red fluorescence signals (Fig. S21†). For the *E. coli* biofilms, red fluorescence signals can be observed only in the CLSM images of the biofilms treated with IBDPPy-PBA or IBDPPy-Ph under light irradiation (Fig. 5F and S22†). Furthermore, the ROS generation capacities of IBDPPy-Ph toward mature biofilms were analyzed with CLSM. The ROS generation in *S. aureus* biofilms was monitored using 2′,7′-dichlorofluorescin diacetate (DCFH-DA) as the probe. The biofilms exhibit strong green fluorescence after treatment with IBDPPy-Ph under green light irradiation (Fig. S23†), whereas the biofilms treated with phosphate buffered saline (PBS) or IBDPPy-Ph without irradiation show negligible fluorescence (Fig. S24†). The imaging results are consistent with the MTT assays, intuitively proving that IBDPPy-Ph could efficiently inhibit biofilm formation and eliminate mature biofilms of both *S. aureus* and *E. coli*.

3.5. *In vivo* evaluation of the antibacterial effects

Inspired by the good *in vitro* activities of IBDPPy-PBA and IBDPPy-Ph against bacteria, *in vivo* evaluation of antibacterial effects was carried out using a *S. aureus*-infected skin wound model (Fig. 6A). All animal procedures were performed in accordance with the Guidelines for Care and Use of Laboratory Animals of Changchun Institute of Applied Chemistry, Chinese Academy of Sciences, and approved by the Animal Ethics Committee of Changchun Institute of Applied Chemistry, Chinese Academy of Sciences (Approval no. 20220005). After wounds with diameters of about 12 mm were made on the backs of mice, the mice underwent 1-day infection treatment with *S. aureus* (10^7 CFU mL^{-1}, 50 μL) to form biofilms. The mice with infected wounds were divided into 5 groups randomly and subjected to treatments separately. PBS

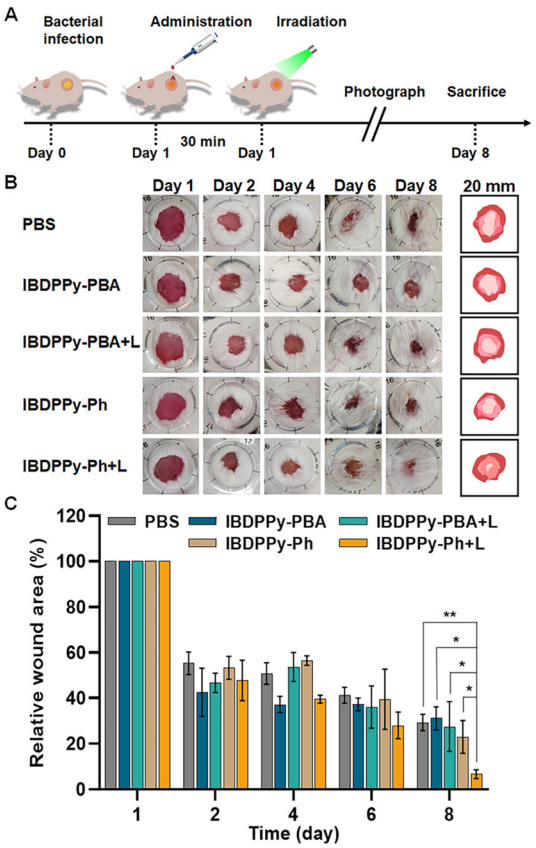

Fig. 6 Evaluation of the antibacterial effects of the BODIPYs *in vivo*. (A) Schematic illustration of the *S. aureus* infected mouse model and the therapeutic process with IBDPPy-PBA and IBDPPy-Ph as the PSs under green light irradiation (18 mW cm^{-2}). (B) Photographs of *S. aureus* infected wounds after different treatments for 8 days and the schematic diagrams of the wound-healing processes. (C) The changes in wound areas during the treatments with PBS, 30 μM IBDPPy-PBA, or IBDPPy-Ph under dark conditions or green light irradiation. *$p < 0.05$ and **$p < 0.01$.

(50 μL), IBDPPy-PBA (30 μM, 50 μL) and IBDPPy-Ph (30 μM, 50 μL) were dripped on the wounds. After 30 min of co-incubation, the mice treated with IBDPPy-PBA and IBDPPy-Ph were exposed to green light irradiation (18 mW cm^{-2}) for 10 min (abbreviated as IBDPPy-PBA + L and IBDPPy-Ph + L) or dark conditions (abbreviated as IBDPPy-PBA and IBDPPy-Ph). The photographs of the infected wounds were constantly taken day by day during the wound-healing process (Fig. 6B and S25†). The wound areas gradually decreased with the evolution of the healing process, as shown in Fig. 6C. The wounds in the IBDPPy-Ph + L group exhibit smaller wound areas than those in other groups on the 8th day, revealing the potent antibacterial activity of IBDPPy-Ph *in vivo* under green light irradiation. The healing rates of the wounds in the PBS, IBDPPy-PBA, IBDPPy-PBA + L, IBDPPy-Ph, and IBDPPy-Ph + L groups are 73.3%, 63.3%, 80.3%, 80.8%, and 94.4%, respectively. The mice were sacrificed on the 8th day, and then the wound tissues were isolated to assess the tissue infection status by hematoxylin and eosin (H&E) staining and bacterial counts on Luria–Bertani (LB) agar plates. There is nearly no bacterial colony observed on the LB agar plates of the IBDPPy-Ph + L group (Fig. S26†). In addition, there are more blood vessels and fewer inflammatory cells in the H&E staining image of the IBDPPy-Ph + L group than in other groups (Fig. S27†), showing that the infected wound tissues treated with IBDPPy-Ph and light irradiation have a better tissue recovery effect. These results indicate that IBDPPy-Ph under irradiation can significantly promote the healing of the infected wounds.

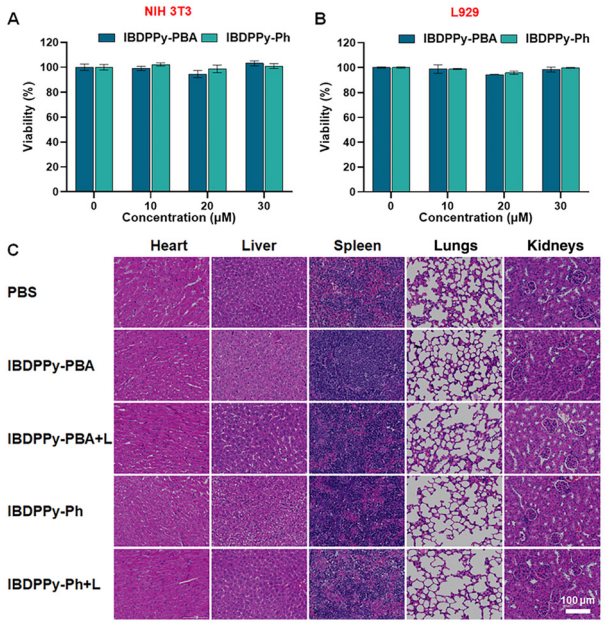

Fig. 7 Cytotoxicity assessment of the BODIPYs. Viabilities of (A) NIH 3T3 and (B) L929 cells incubated with different concentrations of IBDPPy-PBA or IBDPPy-Ph. (C) H&E staining images of different organs (heart, liver, spleen, lungs, and kidneys) from mice after treatments with IBDPPy-PBA or IBDPPy-Ph with or without green light irradiation. Scale bar is 100 μm.

Finally, the cytotoxicity of IBDPPy-PBA and IBDPPy-Ph was evaluated by MTT assays using mouse fibroblast (NIH 3T3 and L929) cells. As shown in Fig. 7A and B, the viabilities of NIH 3T3 and L929 cells incubated with 30 μM IBDPPy-PBA or IBDPPy-Ph changed insignificantly. Besides, the body weights of the mice during the wound-healing processes were recorded, which showed a rising trend during the treatments (Fig. S28†). The major organs (heart, liver, spleen, lungs, and kidneys) of mice were collected and stained with H&E for histological analysis on the 8th day after treatments. There was no obvious histological change or inflammatory region observed in the H&E staining images of the organs (Fig. 7C). Moreover, the hemolysis ratios for IBDPPy-PBA and IBDPPy-Ph (10 μM) are at a safe level (Fig. S29 and S30†). These results verify the good biocompatibility of IBDPPy-PBA and IBDPPy-Ph.

4. Conclusions

In summary, 4 BODIPYs with targeting or positively charged groups were synthesized and evaluated. The *in vitro* antibacterial activities prove that the functional groups of the BODIPYs have significant impact on their photodynamic antibacterial effects. IBDPPy-Ph containing a positive charge shows excellent antibacterial activity against *S. aureus* and *E. coli*, and possesses the ability to inhibit biofilm formation and eliminate mature biofilms under irradiation. IBDPPy-PBA with a targeting group exhibits similar anti-planktonic bacterial activity and inhibition effects toward biofilm formation to IBDPPy-Ph, but it can only eliminate the mature biofilms formed by *E. coli* under irradiation. Interestingly, IBDPPe-PBA reveals selective antibacterial activity against *S. aureus* under irradiation, which may be due to the ample PBA receptors on G+ bacterial membranes. IBDPPy-Ph can successfully inhibit *S. aureus* infections and promote infected wound healing. Overall, this study emphasizes the significance of the design and application of efficient photodynamic antibacterial agents.

Conflicts of interest

There are no conflicts to declare.

Acknowledgements

This work was supported by the National Natural Science Foundation of China (Project no. 52003267 and 51973214) and the Natural Science Foundation of Jilin Province (Project no. YDZJ202101ZYTS027).

References

1 R. C. MacLean and A. San Millan, *Science*, 2019, **365**, 1082–1083.

2 K. Guo, M. Zhang, J. Cai, Z. Ma, Z. Fang, H. Zhou, J. Chen, M. Gao and L. Wang, *Small*, 2022, **18**, 2108030.
3 S. Guo, Q. Huang, Y. Chen, J. Wei, J. Zheng, L. Wang, Y. Wang and R. Wang, *Angew. Chem., Int. Ed.*, 2021, **60**, 618–623.
4 S. Khalid, A. Gao, G. Wang, P. K. Chu and H. Wang, *Biomater. Sci.*, 2020, **8**, 6840–6857.
5 H. Guo, S. Huang, A. Xu and W. Xue, *Chem. Mater.*, 2022, **34**, 2655–2671.
6 L. Zheng, J. Li, M. Yu, W. Jia, S. Duan, D. Cao, X. Ding, B. Yu, X. Zhang and F.-J. Xu, *J. Am. Chem. Soc.*, 2020, **142**, 20257–20269.
7 Y. Feng, C. Coradi Tonon, S. Ashraf and T. Hasan, *Adv. Drug Delivery Rev.*, 2021, **177**, 113941.
8 J. Sun, M. Li, M. Lin, B. Zhang and X. Chen, *Adv. Mater.*, 2021, **33**, 2104402.
9 Y. Sun, H. Qin, Z. Yan, C. Zhao, J. Ren and X. Qu, *Adv. Funct. Mater.*, 2019, **29**, 1808222.
10 U. Ndagi, A. A. Falaki, M. Abdullahi, M. M. Lawal and M. E. Soliman, *Biomater. Sci.*, 2020, **10**, 18451–18468.
11 M. Wu, C. Chen, Z. Liu, J. Tian and W. Zhang, *Acta Biomater.*, 2022, **142**, 242–252.
12 D. Xu, C. Zhou, C. Zhan, Y. Wang, Y. You, X. Pan, J. Jiao, R. Zhang, Z. Dong, W. Wang and X. Ma, *Adv. Funct. Mater.*, 2019, **29**, 1807727.
13 Z. Zhang, Y. Wang, W. Teng, X. Zhou, Y. Ye, H. Zhou, H. Sun, F. Wang, A. Liu, P. Lin, W. Cui, X. Yu, Y. Wu and Z. Ye, *Biomaterials*, 2021, **274**, 120853.
14 X. Wu, M. Yang, J. S. Kim, R. Wang, G. Kim, J. Ha, H. Kim, Y. Cho, K. T. Nam and J. Yoon, *Angew. Chem., Int. Ed.*, 2022, **61**, e202200808.
15 M. R. Hamblin, *Curr. Opin. Microbiol.*, 2016, **33**, 67–73.
16 J. J. Foti, B. Devadoss, J. A. Winkler, J. J. Collins and G. C. Walker, *Science*, 2012, **336**, 315–319.
17 H. Hu, H. Wang, Y. Yang, J.-F. Xu and X. Zhang, *Angew. Chem., Int. Ed.*, 2022, **61**, e202200799.
18 Y. Li, L. Wang, H. Liu, Y. Pan, C. Li, Z. Xie and X. Jing, *Small*, 2021, **17**, 2100756.
19 J. Zhu, J. Tian, C. Yang, J. Chen, L. Wu, M. Fan and X. Cai, *Small*, 2021, **17**, 2101495.
20 M. Kang, C. Zhou, S. Wu, B. Yu, Z. Zhang, N. Song, M. M. S. Lee, W. Xu, F.-J. Xu, D. Wang, L. Wang and B. Z. Tang, *J. Am. Chem. Soc.*, 2019, **141**, 16781–16789.
21 Y. Bai, Y. Hu, Y. Gao, X. Wei, J. Li, Y. Zhang, Z. Wu and X. Zhang, *ACS Appl. Mater. Interfaces*, 2021, **13**, 33790–33801.
22 F. Le Guern, V. Sol, C. Ouk, P. Arnoux, C. Frochot and T.-S. Ouk, *Bioconjugate Chem.*, 2017, **28**, 2493–2506.
23 E. Lee, X. Li, J. Oh, N. Kwon, G. Kim, D. Kim and J. Yoon, *Chem. Sci.*, 2020, **11**, 5735–5739.
24 J. Zhang, W. Liang, L. Wen, Z. Lu, Y. Xiao and M. Lang, *Biomater. Sci.*, 2021, **9**, 5293–5301.
25 Z.-H. Yu, X. Li, F. Xu, X.-L. Hu, J. Yan, N. Kwon, G.-R. Chen, T. Tang, X. Dong, Y. Mai, D. Chen, J. Yoon, X.-P. He and H. Tian, *Angew. Chem., Int. Ed.*, 2020, **59**, 3658–3664.
26 Y. Zhu, S. Wu, Y. Sun, X. Zou, L. Zheng, S. Duan, J. Wang, B. Yu, R. Sui and F.-J. Xu, *Adv. Funct. Mater.*, 2022, **32**, 2111066.
27 L. Wang, S. Li, J. Yin, J. Yang, Q. Li, W. Zheng, S. Liu and X. Jiang, *Nano Lett.*, 2020, **20**, 5036–5042.
28 A. Galstyan, R. Schiller and U. Dobrindt, *Angew. Chem., Int. Ed.*, 2017, **56**, 10362–10366.
29 J. A. Peters, *Coord. Chem. Rev.*, 2014, **268**, 1–22.
30 S. Liu, B. Wang, Y. Yu, Y. Liu, Z. Zhuang, Z. Zhao, G. Feng, A. Qin and B. Z. Tang, *ACS Nano*, 2022, **16**, 9130–9141.
31 L. Liu, X. Wang, S. Zhu, C. Yao, D. Ban, R. Liu, L. Li and S. Wang, *Chem. Mater.*, 2020, **32**, 438–447.
32 H. Zhou, D. Tang, X. Kang, H. Yuan, Y. Yu, X. Xiong, N. Wu, F. Chen, X. Wang, H. Xiao and D. Zhou, *Adv. Sci.*, 2022, **9**, 2200732.
33 C. Zhao, X. Wang, L. Yu, L. Wu, X. Hao, Q. Liu, L. Lin, Z. Huang, Z. Ruan, S. Weng, A. Liu and X. Lin, *Acta Biomater.*, 2022, **138**, 528–544.
34 S. Wu, C. Xu, Y. Zhu, L. Zheng, L. Zhang, Y. Hu, B. Yu, Y. Wang and F.-J. Xu, *Adv. Funct. Mater.*, 2021, **31**, 2103591.
35 Z. Liu, Q. Wang, W. Qiu, Y. Lyu, Z. Zhu, X. Zhao and W.-H. Zhu, *Chem. Sci.*, 2022, **13**, 3599–3608.
36 X. Su, R. Liu, Y. Li, T. Han, Z. Zhang, N. Niu, M. Kang, S. Fu, D. Wang, D. Wang and B. Z. Tang, *Adv. Healthcare Mater.*, 2021, **10**, 2101167.
37 M. Ye, Y. Zhao, Y. Wang, M. Zhao, N. Yodsanit, R. Xie, D. Andes and S. Gong, *Adv. Mater.*, 2021, **33**, 2006772.
38 A. Kamkaew, S. H. Lim, H. B. Lee, L. V. Kiew, L. Y. Chung and K. Burgess, *Chem. Soc. Rev.*, 2013, **42**, 77–88.
39 H.-Y. Kwon, X. Liu, E. G. Choi, J. Y. Lee, S.-Y. Choi, J.-Y. Kim, L. Wang, S.-J. Park, B. Kim, Y.-A. Lee, J.-J. Kim, N. Y. Kang and Y.-T. Chang, *Angew. Chem., Int. Ed.*, 2019, **58**, 8426–8431.
40 C. Li, Y. Li, Q. Wu, T. Sun and Z. Xie, *Biomater. Sci.*, 2021, **9**, 7648–7654.
41 W. J. Peveler, S. Noimark, H. Al-Azawi, G. B. Hwang, C. R. Crick, E. Allan, J. B. Edel, A. P. Ivanov, A. J. MacRobert and I. P. Parkin, *ACS Appl. Mater. Interfaces*, 2018, **10**, 98–104.
42 Q. Zhao, C. Yin, J. Kang, Y. Wen and F. Huo, *Dyes Pigm.*, 2018, **159**, 166–172.
43 J.-Y. Liu, H.-S. Yeung, W. Xu, X. Li and D. K. P. Ng, *Org. Lett.*, 2008, **10**, 5421–5424.
44 J. Zhao, W. Wu, J. Sun and S. Guo, *Chem. Soc. Rev.*, 2013, **42**, 5323–5351.
45 B. Hao, J. Wang, C. Wang, K. Xue, M. Xiao, S. Lv and C. Zhu, *Chem. Sci.*, 2022, **13**, 4139–4149.
46 W. Hu, T. He, H. Zhao, H. Tao, R. Chen, L. Jin, J. Li, Q. Fan, W. Huang, A. Baev and P. N. Prasad, *Angew. Chem., Int. Ed.*, 2019, **58**, 11105–11111.
47 G. McDonnell and A. D. Russell, *Clin. Microbiol. Rev.*, 1999, **12**, 147–179.
48 Y. Wang, T. S. Corbitt, S. D. Jett, Y. Tang, K. S. Schanze, E. Y. Chi and D. G. Whitten, *Langmuir*, 2012, **28**, 65–70.
49 H. Li, M. Yang, J. S. Kim, J. Ha, J. Han, H. Kim, Y. Cho, J. Wang, K. T. Nam and J. Yoon, *Biomaterials*, 2022, **286**, 121580.

